Droughts across China: drought factors, prediction and impacts

Qiang Zhang[1,2,3], Rui Shi[1,2,3], Vijay P. Singh[4], Chong-Yu Xu[5], Huiqian Yu[6,7], Keke Fan[1,2,3], Zixuan Wu[1,2,3]

1. Key Laboratory of Environmental Change and Natural Disaster, Ministry of Education, Beijing Normal University, Beijing 100875, China;
2. Faculty of Geographical Science, Academy of Disaster Reduction and Emergency Management, Beijing Normal University, Beijing 100875, China;
3. State Key Laboratory of Earth Surface Processes and Resources Ecology, Beijing Normal University, Beijing 100875, China;
4. Department of Biological and Agricultural Engineering and Zachry Department of Civil Engineering, Texas A&M University, College Station, Texas, USA, and National Water & Energy Center, UAE University, Al Ain, UAE;
5. Department of Geosciences and Hydrology, University of Oslo, N-0316 Oslo, Norway;
6. State Key Laboratory of Urban and Regional Ecology, Research Center for Eco-Environmental Sciences, Chinese Academy of Sciences, Beijing, 100085, China;
7. University of Chinese, Academy of Sciences, Beijing, 100049, China.

Correspondence to Qiang Zhang: zhangq68@bnu.edu.cn

Abstract: Drought is a complicated and costly natural hazard, combining the effects of precipitation, air temperature, evapotranspiration, and so on. Identification of critical drought factors is the first step into modelling and forecasting of droughts and hence development of drought mitigation measures (the Standardized Precipitation-Evapotranspiration Index) in both space and time. Here we analyzed the relationship between drought and 23 drought factors, using remote sensing data from 2002-2016. Based on the Gradient Boosting Algorithm (GBM), we found that precipitation and soil moisture had relatively large contributions to droughts. During the growing season, the Normalized Difference Water Index (NDWI) showed a relatively higher importance for drought. However, during the non-growing season, the Snow Cover Fraction (SCF) had larger fractional relative importance for short-term droughts in the Inner Mongolia and the Loess Plateau. We also compared Extremely Randomized Trees (ERT), H2O-based Deep Learning (Deep Learning with H2O, H2O.DL), and Extreme Learning Machine (ELM) for drought prediction at various time scales, and found that the ERT model had the best prediction with R^2>0.72. Based on the Meta-Gaussian model, we quantified the probability of maize yield reduction in the North China Plain under different compound dry-hot conditions. Due to extreme drought and hot conditions, Shandong Province in North China had the highest probability of >80% of the maize yield reduction, and due to the extreme hot conditions, Jiangsu Province in North China had the largest probability of >86% of the maize yield reduction.

Key words: Drought factors; Modelling accuracy; Compound disaster; Prediction; Impacts; Crop yield

1. Introduction

Drought is one of the most complex, costly, and less understood natural disasters, and has a huge impact on water resources, agricultural production, and human health (Dai et al., 2004; Guo et al., 2019; Yu et al., 2019). Generally, four types of droughts have been classified: meteorological drought, agricultural drought, hydrological drought, and socio-economic drought (Wilhite and Glantz, 1985). Agricultural drought occurs due to soil moisture (SM) deficit which adversely affects crop yields (Zhang et al., 2017a; Zhou et al., 2017; Zhang et al., 2019). Recent years witnessed frequent droughts and serious drought risk for crop yield reduction across China (Dalin et al., 2015; Wang et al., 2016; Zhang et al., 2019).It is therefore important to throw a new light on driving factors, prediction, and impacts of drought at the regional scale.

Drought is the combined result of complex interactions amongst precipitation, air temperature, water vapor pressure, and solar radiation (Leng and Hall, 2019), and current drought indices were developed using hydrometeorological variables, such as precipitation, evapotranspiration, SM and so on (Hayes et al., 2007; Yu et al., 2019; Zhang et al., 2018, 2019). The widely-used drought monitoring indices, including the Standardized Precipitation Index (SPI) (McKee et al., 1993), the Standardized Precipitation Evapotranspiration Index (SPEI) (Vicente-Serrano et al., 2010), and Palmer Drought Severity Index (PDSI) (Palmer, 1965) are based on in-situ meteorological observations. In the high-altitude areas, it is difficult to obtain reliable information to evaluate the spatiotemporal patterns of droughts (AghaKouchak et al., 2015) due to the sparse and uneven distributions of meteorological stations. These shortcomings can be overcome by basing drought monitoring indices based on remotely sensed data (AghaKouchak and Nakhjiri, 2012; Sun et al., 2017; Zhang et al., 2019).

Hydrometeorological variables, such as precipitation, SM, air temperature, snow, evaporation, and water storage, can be obtained via remotely sensed datasets and can be used to evaluate the impact of hydrometeorological changes on the occurrence of drought (AghaKouchak et al., 2015; Lillesand et al., 2015). Actually, several remote sensing data-based drought monitoring indices have been developed, including the Normalized Differential Vegetation Index (NDVI) (Rouse et al., 1974), Normalized Difference Water Index (NDWI) (Gao, 1996), Normalized Difference Drought Index (NDDI) (Gu et al., 2007), and Land Surface Water Index (LSWI) (Xiao et al., 2004). These remote sensing data-based drought indices have established linkages between drought factors and occurrences of droughts, and help onitor droughts by the evaluation of changes in these factors. Drought factors behave in different ways at the regional scale and hence the right selection of these factors (or variables) is critical for regional drought monitoring. Therefore, it is a essential to identify critical drought factors that have significant impacts on the occurrence of droughts at the regional scale.

Snow is one of the important factors affecting SM changes and hence the occurrence of drought. Insufficient snow can also potentially trigger the occurrence of agricultural drought (AghaKouchak et al., 2015). Analyses of relations between summer maximum NDVI and snow cover in spring showed a strong correlation between the peak NDVI value in summer and spring snow (Verbyla, 2015). Therefore, the impact of snow on SM changes should not be overlooked. Actually, the remotely sensed snow data have been widely used in drought monitoring (Molotch and Margulis, 2008; Guan et al., 2013; Faiz et al., 2020). Although snow cover data has been used as input into hydrological models for modelling of runoff changes, it has not been used for monitoring agricultural droughts. Therefore, it is still a challenge to understand the impact of snow on drought. In this study, we used the remotely sensed snow data to establish the linkage between snowfall-related variables and agricultural droughts.

Other natural factors also influence drought and can be used to monitor drought conditions. Hence, the proper selection of drought factors is important to evaluate drought characteristics, and proper models and algorithms are crucial for the estimation and assessment of drought conditions but the reliability and accuracy of current models are not adequately known (Alizadeh and Nikoo, 2018). Compared with traditional models, machine learning methods can better analyze the hierarchical and nonlinear relationships between independent variables and dependent variables (Belayneh et al., 2014; Guzmán et al., 2018). Park et al. (2016) compared three machine learning methods for SPI-based drought prediction based on the selected drought factors. However, they focused only on the impacts of drought factors on drought during growing seasons but did not analyze the performance of drought factors during non-growing seasons. Feng et al. (2019a) did SPI-based drought prediction with relatively important remotely sensed drought factors. However, drought responds differently to drought factors, such as vegetation (Park et al., 2016).

To better monitor drought, it is necessary to compare drought response to drought factors. In addition, the performances of machine learning-based models based on drought factors are different at regional scales and the accuracy of models remains to be investigated. The occurrence of drought threatens crop yield so it is important to assess the risk of drought-induced crop yield reduction. Besides, the accuracy of drought assessment directly affects the reliability of assessment of the drought-induced crop yield reduction risk. In this study, we aim to quantify the risk of drought-induced crop yield reduction using the SPEI predicted from the optimal model. Ray et al. (2015) found that compound disasters caused by the simultaneous occurrence of drought and heatwave had greater impacts on crop yield than had an individual extreme drought event. Feng et al. (2019b) used a multivariate joint probability model to assess the risk of maize yield reduction in major countries around the world under compound dry-hot events. The North China Plain (NCP) is the largest producer of crop yields, particularly maize production, so it is important to evaluate the risk of maize yield reduction due to the compound dry-hot condition.

Therefore, the major objective of this study is to identify the principal factors influencing the occurrence of drought using machine learning methods. Besides, we also attempt to address the drought prediction using different models and evaluate the risk of drought-induced maize yield reduction. Specifically, the objectives of this study are to: (1) assess the relative importance of different drought factors derived from satellite data products on drought characteristics at different time scales; (2) compare the predictive performances of different machine learning models based on different drought factors; and (3) quantify the risk of drought-induced maize yield reduction in NCP under different compound dry-hot conditions.

2. Data

2.1 In-situ meteorological observation data and maize production data

Daily precipitation and average air temperature data from 2474 meteorological stations (Fig. 1) for a period from 1960 to 2014 were obtained from the National Climate Center of the China Meteorological Administration. The annual maize production data of Jiangsu, Anhui, Shandong, Hebei, and Henan provinces for a period from 1961 to 2016 were sourced from the National Bureau of Statistics (http://data.stats.gov.cn/easyquery.htm?cn=E0103).

2.2 Remote sensing data

The remote sensing data at monthly scale for a period from 2002 to 2016 were sourced from the Moderate Resolution Imaging Spectroradiometer (MODIS) sensor by the National Aeronautics and Space Administration (NASA) (https://search.earthdata.nasa.gov/search). The land surface reflectance data (bands 1-7) were from MOD09A1, and the Potential Evapotranspiration (PET) and Evapotranspiration (ET) data were from MOD16A2. The temporal and spatial resolutions are 8 days and 500 m, respectively. The Land Surface Temperature (LST) and the Normalized Difference Vegetation Index (NDVI) were derived from MOD11A2 and MOD13A3, respectively, with a spatial resolution of 1 km. The Snow Cover Fraction (SCF) data was obtained from MOD10A2, and the temporal and spatial resolutions were 8 days and 500 m, respectively. Here we used the SCF data for only the non-growing season (November to March of the subsequent year) for further analysis. For the MODIS products with a time resolution of 8 days and a spatial resolution of 500 m, we converted the time and space scale to 1 km and monthly scale for further analysis (Park et al., 2016).

The monthly precipitation data from TRMM satellite sensors were sourced from https://disc.gsfc.nasa.gov/mirador-guide with a spatial resolution of 25 km during a period from 2002 to 2016. In addition, the TRMM data were calculated at time scales of 1, 3, 6, 9 and 12 months to analyze the lag between drought and precipitation.

2.3 Global Land Data Assimilation Systems (GLDAS) data

The monthly SM data with a spatial resolution of 25 km for a period from 2002 to 2016 was sourced from https://ldas.gsfc.nasa.gov/gldas/gldas-get -data. The SM data were obtained by the Noah model of GLDAS (Global Land Data Assimilation Systems). Similarly, we calculated the SM data at time scales of 1, 3, 6, 9 and 12 months to analyze the lag between drought and SM changes. The time intervals of data were subdivided into two parts, i.e. growing season and non-growing season. The period of April to October of each year was taken as the growing season (Park et al., 2016), and the other months were taken as the non-growing season. We used the maximum-minus-minimum scaling ratio (from 0 to 1) to scale all the variables for each month for the period from 2000 to 2012 to identify the variability of weather and climate from the spatial heterogeneity (Kogan, 1995; Lu et al., 2019) (Table 1). In order to compare NDWI6, only LSWI was standardized to eliminate the influence of data scale. The equations for different drought factors are listed in Table 1, where "ρ" _band 2, 5, 6, and 7, respectively, represent the land surface reflectance recorded in the 2, 5, 6, and 7 bands of the MOD09A1 product. The PSMD was estimated from January of each year ($i = 1$), and the $PSMD_{i-1}$ was reset to 0 for the subsequent year to avoid the carryover of the previous year's soil water deficit (Stewart, 2017). Then, 23 variables including TCI, VCI, SMCI, PCI, SCF, ET, NMDI, NDWI5-7, NDDI5-7, SM3-12, TRMM3-12, PSMD, LSWI were obtained (Table 1).

3. Methods

We first analyzed the impact of drought factors on the occurrence of SPEI-based droughts and then evaluated the accuracy of drought prediction using different machine learning-based models. Thereafter, we evaluated the risk of maize yield reduction due to compound dry-hot conditions. The procedure of analysis is shown in Fig. S1 of Supplementary materials. The first step was to cluster the meteorological stations (Supplementary materials, Fig. S2) and seven sub-regions were identified (Supplementary materials, Fig. S3) using the FCM (Fuzzy C-means) algorithm. Then we used the Gradient Boosting Algorithm (GBM) to analyze the response of drought to different factors at different time scales. Meanwhile, three machine learning-based models were developed to model and predict droughts at different time scales. Finally, the meta-Gaussian model was used to evaluate the risk of maize yield reduction due to the compound dry-hot conditions in North China.

3.1 Calculation of SPEI, STI (Standardized Temperature Index), SCI (Standardized

Crop Yield Index)

In this study, we used the Penman-Monteith equation to evaluate potential evapotranspiration. The monthly water balance was computed, based on the difference between monthly precipitation and monthly potential evapotranspiration. The log-logistic probability distribution model was used to standardize the monthly water balance to obtain SPEI (Vicente-Serrano et al., 2010). The SPEI was computed at different time scales such as 1, 3, 6, 9 and 12 months during 1960-2014 to evaluate the lag between precipitation, SM, and other factors and drought. The calculation of SPEI was based on the R software package at https://cran.r-project.org/web/packages/SPEI/. To evaluate the risk of maize yield reduction due to the dry-heat compound hazard, the monthly average air temperature was used to develop the Standardized Temperature Index (STI) (Zscheischler et al., 2014). The Standardized Crop yield Index (SCI) was developed using the Normal Quantile Transformation (NQT) on the maize yield data (Feng et al., 2019b).

3.2 Fuzzy C-means (FCM) clustering

Fuzzy C-means algorithm is one of the widely-used fuzzy clustering algorithms (Dunn, 1973) and was improved by Bezdek (1981). Let $\mathrm{X} = \{\mathrm{X}_1, \mathrm{X}_2, \mathrm{X}_3, \cdots, \mathrm{X}_\mathrm{n}\}$ be a set of data in space; and P be the number of different clusters: $\mathrm{P} = \{\mathrm{C}_1, \mathrm{C}_2, \cdots, \mathrm{C}_\mathrm{m}\}$, where $\mathrm{m} \geq 2$. The clustering procedure based on the FCM algorithm is an iterative procedure that requires solving the minimum value of the objective function in Eq. (1) (Bezdek, 1981; Rao and Srinivas, 2006):

$$J_m(U,V:X) = \sum_{i=1}^{m}\sum_{j=1}^{n}\left(u_{ji}\right)^k d^2(X_j,V_i) \tag{1}$$

subject to the following conditions:

$$\sum_{i=1}^{m} u_{ji} = 1 \qquad \forall j \in \{1,\cdots,n\} \tag{2}$$

$$0 < \sum_{i=1}^{m} u_{ij} < n \quad \forall i \in \{1,\cdots,m\} \tag{3}$$

where $V = \{V_1, V_2, \cdots, V_m\}$ represents the center of each cluster; $d^2(X_j, V_i)$ represents the distance between X_j and V_i; and u_{ji} represents that the *j*th data belongs to the *i*th cluster membership. In the FCM model, Eqs. (4) and (5) are used to calculate the new cluster centers and the degree of membership, respectively, and are brought into Eq. (1) to update the objective function:

$$V_i = \frac{\sum_j^n \left(u_{ji}\right)^k X_n}{\sum_j^n \left(u_{ji}\right)^k} \quad for\ 1 \le i \le m \tag{4}$$

$$u_{ji} = \frac{\left(\frac{1}{d^2(X_j,V_i)}\right)^{1/(k-1)}}{\sum_i^m \left(\frac{1}{d^2(X_j,V_i)}\right)^{1/(k-1)}} \quad for\ 1 \le i \le m, 1 \le j \le n \tag{5}$$

When the results of the two objective functions is small enough, the iteration is stopped, and the category to which each data set belongs to is then obtained. To determine the optimal number of clusters, four cluster validity indicators were selected for verification in this study (Table 2). The larger the value of MPC, SIL and SIL.F (Table 2), the better the number of clusters. The smaller the XB value, the better the number of selected clusters.

3.3 Gradient Boosting Model (GBM)

GBM is a widely-used ensemble learning method, which can be used to develop classification models and also regression analysis (Friedman, 2001; Friedman, 2002).

The ensemble learning method can be used for prediction based on multiple classification or regression models. Through the ensemble of multiple tree models, the prediction accuracy can be greatly improved. In addition, the model can also be used to rank the variables according to their importance as predictor variables, which can help eliminate unimportant feature variables (Tuv et al., 2009).

Comparison of different ensemble learning models indicated that the probability of selecting a single sample for each training of the boosting model was not equal, and the probability of selecting the wrong sample was high, while the bagging model trained each model by sampling with equal probability. The boosting model used this sample selection method to attach more importance to the training of samples with each newly-created model to minimize the average loss function of the training model (Zhang and Haghani, 2015). The GBM improves the modelling accuracy by the reduction of loss function largely via the integration of various models strategically. To analyze the relative importance of different variables for drought, the Gini index was used and was quantified by the decrease in the impurity of tree nodes during the modeling process (Machado, et al., 2015; Rao et al., 2019). The impurity of a certain node *t* can be obtained as (Zhang et al., 2020):

$$i(t) = \frac{\sum_{m \in \delta(t)} w_m f_m (y_m - \bar{y}(t))^2}{\sum_{m \in \delta(t)} w_m f_m} \tag{6}$$

where δ(t) denotes the training samples located at node *t*; w_m and f_m denote the proportional weight and frequency weight of the regression result of *m*, respectively; y_m denotes the dependent variable corresponding to *m*; $\bar{y}(t)$ denotes the average of dependent variables of all samples in node *t*. The separation principle *s* of node *t* was to maximize $\Delta i(s,t)$, and the calculation method of $\Delta i(s,t)$ was as follows:

$$\Delta i(s,t) = i(t) - \sum_{n \in t} P_n i(t_n) \tag{7}$$

t_n denotes the *n*th child node of node *t*; P_n denotes the proportion of samples in node *t* that were subdivided into the *n*th child node. The Gini indices of all nodes of each drought factor were summed and standardized according to the number of trees. Then we obtained the relative importance of each drought factor. The larger the value, the greater the contribution of each drought factor to the development of the integrated tree model, and the greater the impact of the drought factor on the dependent variable.

3.4 Machine learning-based prediction model

3.4.1 Extremely Randomized Trees (ERT)

Geurts et al. (2006) proposed the Extremely Randomized Trees (ERT), which is a tree-based ensemble learning algorithm that can be used to solve unsupervised classification and regression problems. When compared to other tree-based methods, this algorithm splits nodes by randomly selecting attributes and split points during the growth of each tree (Marée et al., 2007). Particularly, given comparison to the bagging model-based random forest model, ERT has two main advantages: (1) The random forest model depends the bagging model for random selection of samples, while ERT involves all samples in the development and growth of trees to improve the accuracy of the model to a certain extent; (2) random sampling and selection of variable features during the tree node classification, which can help get more effective data reasoning (Gupta et al., 2019). The randomness of such modeling effectively improves the overall predictive performance of the model. Therefore, here we used ERT for modeling and regression prediction in the tree-based integrated algorithm model, and compared the prediction performance of other machine learning-based methods.

3.4.2 Deep Learning with H2O (H2O.DL)

The H2O-based deep learning model uses a Multi-Layer Feedforward (MLF) neural network for predictive modeling, which can be used for both classification and regression analysis (Candel et al., 2016). MLF includes multiple neural layers, i.e. input layer, hidden layer, and output layer. The middle layer involves multiple hidden layers and contains multiple non-linear transfer functions. Feedforward refers to the sequential conversion of input information in one direction, that is, from front to back, without repeated connections (Pumsirirat and Yan, 2018). Deep learning models can extract useful information from original data to a large extent, and show high performance in processing complex data (Candel et al., 2016). Here we used the R platform to develop an H2O-based deep learning model (Zambrano et al., 2018).

3.4.3 Extreme Learning Machine (ELM)

The ELM was proposed by Huang et al. (2006) and includes two steps of computation, i.e. construction of the hidden layer random mapping feature based on randomly generated neurons, and solving the weight between the hidden layer and the output layer (Huang et al., 2014). When compared to the traditional neural network models such as support vector machines, ELM has faster calculation speed, fewer setting parameters, and is easier to use (Rajesh and Prakash, 2011). Besides, when compared to deep learning models, the ELM has a single hidden layer and this single feedforward neural network greatly improves the calculation speed of the model.

3.4.4 Model verification

To avoid over-fitting, 75% of the samples were randomly selected as training samples, and 25% of the samples were for model verification. In addition, a ten-fold cross-validation method was used to verify the model. The cross-validation method was accepted to ensure the reliability and robustness of the model (Rodriguez et al., 2009). The model performance was evaluated, based on R^2 (coefficient of determination), RMSE (root mean-square error), and MAE (the mean absolute error) (Li et al., 2017).

3.5 Meta-Gaussian model

The meta-Gaussian model can express the degree of correlation between variables through marginal distributions (Kelly and Krzysztofowicz, 1997). The three-variable meta-Gaussian model integrates the three variables of temperature, drought, and crop yield, which can assess the risk of crop yield reduction under the compound dry-hot condition. Let $\mathrm{X} = [\mathrm{X}_1, \mathrm{X}_2]$ be two standardized random variables, and the corresponding conditional distribution function Y is (Wilks, 2011):

$$\mathrm{Y}|\mathrm{X}_1, \mathrm{X}_2 \sim \mathrm{N}(\mu_{\mathrm{Y}|\mathrm{X}_1,\mathrm{X}_2}, \Sigma_{\mathrm{Y}|\mathrm{X}_1,\mathrm{X}_2}) \tag{8}$$

where $\mu_{Y|X_1,X_2}$ is the mean value of Y under the condition of X, and $\sum_{Y|X_1,X_2}$ is the covariance matrix, and can be obtained by Eqs. (9) and (10), respectively:

$$\mu_{Y|X_1,X_2} = \mu_y + \sum_{yx}\sum_{xx}{}^{-1}\,(x - \mu_x) \quad (9)$$

$$\sum_{Y|X_1,X_2} = \sum_{yy} - \sum_{yx}\sum_{xx}{}^{-1}\sum_{yx} \quad (10)$$

where μ_y and μ_x denote the mean value of variable Y and vector X, respectively. $\sum_{yx}$, $\sum_{yy}$, $\sum_{xx}$ denote the covariance matriices of X and Y. In this study, SPEI and STI were represented by X_1 and X_2, respectively, and SCI by Y.

4. Results

4.1 Results by clustering analysis

China is dominated by complicated topographic features and various climate types. Different topographies and climate conditions lead to different responses of drought to drought factors. Here we used the FCM clustering algorithm to classify climate types across China. The latitude, longitude, altitude, and average monthly SPEI at 2474 stations were considered in climatic regionalization (Supplementary materials, Fig. S2). Based on Fig. S2, the optimal number of clusters was determined to be 7, and the spatial distribution of meteorological stations of the initial clusters is shown in Fig. S3a. Due to the overlap of some points on the boundaries of each cluster, we readjusted the clusters and the final cluster results are shown in Figs. S3b and S3d. Due to the sparse distribution of meteorological stations Ii the Northwest and the Qinghai-Tibet Plateau, the number of stations in A and C districts was significantly less than in other areas (Fig. S3c).

4.2 Distribution of variables in each cluster

Here we used the probability distribution, scatter plots, and box plots to analyze the distribution of variables between different clusters from 2002 to 2016 and the relationship between variables in this study. Fig. S4 shows the distribution of the variables of ET, SMCI, LSWI, NDDI5, NDDI6, NDDI7, PSMD, SCF and SPEI in the 7 clusters and the correlation between different variables. The insets along the diagonal line show the probability distribution of a single variable in each cluster. The insets within the upper triangle show the contour maps and the correlation coefficients obtained by the two-dimensional density between different variables, while the insets within the lower triangle illustrate the scatter plots for two variables, where the red parts illustrate the high-density points, and the blue parts indicate the area where the number of points is sparsely distributed. The box plot in the last column shows the distribution of the effective value of the variable in different clusters. The insets along the diagonal direction indicate that for a single variable, the distribution of the high and low concentration intervals in different clusters is basically the same. Comparison of insets within the upper triangle area in Fig. S4 indicates the sparse and sporadic distribution of contour density between ET, SMCI and NDDI5, NDDI6, and NDDI7. NDDI5, NDDI6, and NDDI7 obtained by the land surface reflectance had high correlation and a linear relationship. However, the scatter points had low concentration, showing the influence of complexity of the ground features on land surface reflectance. As for SCF, the areas with more snow cover are concentrated in clusters A and B, which are the northwest and northeast regions, respectively. SCF has a strong correlation with vegetation indices, such as LSWI, NDDI5, NDDI6, NDDI7, etc., and the strongest correlation was between SCF and LSWI, i.e. 0.404. Bajgain et al. (2015) found that LSWI captured the signal of SM drop earlier than did NDVI and other indices. Therefore, LSWI respond to SM changes due to snow variations and hence indicated drought conditions. Meanwhile, stronger correlation between LSWI and SCF was found in regions with low SCF, indicating greater impacts of low snow coverage on vegetation. In general, except for PSMD and ET, each variable showed a certain positive correlation with SPEI, indicating that each variable identified drought characteristics to a certain extent, and can be used for monitoring and evaluation of droughts.

Fig. S5 shows the distribution of variables NDWI5, NDWI6, NDWI7, NMDI, PCI, TCI, VCI and SPEI in the 7 clusters and the correlation amongst these variables. It can be seen from the insets along the diagonal direction that except for NDWI6 and NDWI7, the probability distributions of variables in different clusters were basically the same. Contours of the probability density of variables in the insets of the upper triangle illustrated higher correlations between NDWI5, NDWI6 and NDWI7. Specifically, the correlation between NDWI6 and NDWI7 iwa as high as 0.9. Besides, we can also observe higher correlation between TCI and vegetation indices, such as NDWI5, NDWI6, and NDWI7. It was due to the fact that land surface temperature (LST) reflected SM conditions of the top soil that can directly influence crop yield (Sayago et al., 2017). Except for VCI, almost all variables had positive correlations with SPEI. Scatter points of NMDI, PCI, and SPEI were concentrated in the regions dominated by lower SPEI values. Scatter plots indicated no evident linear relations between variables but these variables had a certain relationship with SPEI, showing that these variables reflected drought conditions to a certain degree. Therefore, how to select the right variables to characterize drought is still challenging.

4.3 Relative importance of drought factors for different time scale droughts

In order to identify the ability of different drought factors to monitor drought in different regions and at different times, the relative importance of different variables for drought in the growing season and the non-growing season were analyzed. We evaluated the relative importance of 23 variables for drought at different time scales during the period from 2002 to 2016 based on the GBM, and 10 most important factors for drought were screened out. Fig. 2 demonstrates the relative importance of the top 10 variables calculated in the non-growing season (Figs. 2a1, b1, c1, d1, e1) and the variables that appear most frequently in each cluster (Figs. 2a2, b2, c2, d2, e2). It can be seen from Fig. 2 that TRMM and SM at different time scales were the most important variables in drought monitoring, particularly for the long-term drought of 6-month, 9-month and 12-month time scale SPEIs. The SM9 showed relatively high importance for 12-month time scale SPEI in each cluster (Fig. 2e1), indicating that the cumulative SM had a certain lag effect on long-term drought in each region, and the lag time was 3 months. Specifically, in clusters F and G, the relative importance of TRMM6, TRMM9, and TRMM12 for SPEI6, SPEI9, and SPEI12 was higher than that of SM6, SM9, and SM12, respectively, implying that precipitation changes meant more for droughts than for SM changes. In addition to SM and precipitation, TCI was also an important variable to characterize drought. The relative importance of TCI decreased as the time scale increased, and it was more suitable for monitoring short-term drought (from 1-month to 3-month SPEI). In clusters B, C, D, and E, SCF showed high relative importance for SPEI1 and SPEI3. SCF was also the third most important variable for SPEI1 in cluster C, and the relative importance of SCF for SPEI1 in cluster D also reached as high as 10%, indicating that the impact of snow cover changes on drought in the non-growing season cannot be ignored. It is one of the important variables for evaluating and monitoring drought. NDWI5, NDWI6, NDWI7, NDDI5, NDDI6, NDDI7, NMDI and LSWI can be used to monitor drought from the viewpoint of vegetation water content (Gao, 1996; Wang and Qu, 2007; Zhou et al., 2017). During the non-growing season, these variables only showed high relative importance for short-term drought (SPEI1). In cluster E, the relative importance of NDDI7 for SPEI1 reached 32%, and the relative importance of NDWI7 in cluster B almost reached 20%. In general, the relative importance of NDWI7 was higher than that of NDWI5 and NDWI6 for drought, and the importance of NDDI7 was higher than that of NDDI5 and NDDI6. In particular, in cluster A, LSWI showed a relatively high importance for SPEI at different time scales, being up to 16%. It showed that LSWI was an important variable in evaluating droughts in Northwest China.

Fig. 3 illustrates top 10 variables that showed the highest importance for different time scales of drought during the growing season in different clusters (Figs. 3a1, b1, c1, d1, e1) and also drought factors that occurred most frequently in different clusters (Figs. 3a2, b2, c2, d2, e2). When compared to the non-growing season, the variables related to the vegetation index showed relatively higher importance for drought during the growing season. The relative importance of NDWI7 for SPEI3, SPEI6, SPEI9, and SPEI12 basically reached as high as 50%. NDWI7 was highly sensitive to changes in drought intensity (Gu et al., 2007). NDWI6 showed a relatively remarkable importance for SPEI1 and can be used in monitoring of short-term droughts. TCI was an important variable for monitoring short-term drought in each cluster. As the time scale of SPEI increased, the relative importance of TCI gradually decreased. Therefore, TCI was more sensitive to the short-term drought (Zhang and Jia, 2013). In addition to NDWI7, precipitation and SM were still important variables for drought monitoring. SM3, SM6, and SM9 showed relatively high importance for SPEI6, SPEI9, and SPEI12 in each cluster, which means that there was a time lag effect between SM and drought, and the lag period was 3-6 months. In clusters E, F, and G, TRMM3 and TRMM6 showed relatively higher importance for SPEI6 and SPEI9, respectively, and there was a three-month time lag between the response of drought and precipitation. Meanwhile, the relative importance of precipitation for drought was higher than that of SM, and drought was highly sensitive to precipitation changes. Comparatively, the relative importance of ET for drought during the non-growing season was higher than that during the growing season.

When compared to the relative importance of drought factors during different seasons, we found remarkable differences of drought factors in the identification of droughts. During the growing season, NDWI7 and 1-, 3-, 6-, 9- and 12-month time scale accumulated SM and TRMM were important factors for monitoring droughts. TCI was an important variable for monitoring short-term drought. During the non-growing season, the sensitivity of vegetation for drought decreased with the increasing time scale. SM at the time scales of 1, 3, 6, 9 and 12 months and TRMM were important factors for monitoring droughts at different time scales. And SCF, TCI, NDWI7 and NDDI7 were indispensable variables for monitoring short-term drought.

4.4 Prediction accuracy of models for droughts

We compared the predictive performance of three models, i.e. ELM, ERT, and H2O.DL, based on different drought factors identified in the above sections. R^2, MAE, and RMSE were used to evaluate the predictive performance.

4.4.1 Performance evaluation of models

We used the GBM model to evaluate the relative importance of drought factors for SPEI1-12 and 23 variables in each model were ranked based on relative importance. The top ten important variables were included in analyses. Besides, different machine learning-based models were used to develop models based on the screened and original drought factors, in order to verify the important variables and compare the accuracy of machine-learning-based models. Ori-ELM, Ori-ERT, Ori-H2O.DL represent models developed based on the original set of 23 variables, and ELM, ERT, H2O.DL represent models developed based on the screened 10 variables. Fig. S6 shows the fitting performance and reliability of different models for prediction during the non-growing season. We found that the prediction accuracy was constant whether for original or screened variables, indicating convincing screened variables by GBM. The accuracy of the models developed by machine-learning-based methods varied greatly in different clusters. In clusters A and C, the overall accuracy of each model decreased which was the result of the sparse distribution of meteorological stations. Comparison of the accuracy of models showed that the ERT model had the highest prediction accuracy and reliability, followed by the H2O.DL model, and the ELM model had the lowest prediction accuracy. For models performance in cluster G, the R^2 of ERT reached 0.64, which was 0.06 and 0.24 higher than that of H2O.DL and ELM, respectively. In addition, the RMSE and MAE values of ERT remained around 0.41 and 0.46, respectively, and the results of the 10-fold cross-validation were constant. The prediction accuracy of ERT and H2O.DL models varied with time scales of SPEI. As the time scale of SPEI increased, the overall accuracy of the model decreased slightly. The overall accuracy of the ELM model in each cluster was low. In general, the accuracy of the ELM model fluctuated greatly. For example, the prediction accuracy of SPEI6 obtained by ELM in clusters B and E was high, and R^2 of ELM was consistent with the H2O.DL model, which should be attributed to the single hidden layer of the ELM model. Fig. S7 shows the fitting performance and reliability of each model during the growing season. Comparison of the R^2, MAE and RMSE values of different models indicated that the ERT model had the highest prediction accuracy, followed by H2O.DL, and the ELM model had lower prediction accuracy. In cluster B, when the predictor variable was SPEI6, the accuracy of the ERT model was the highest, and the R^2 reached as high as 0.72. The RMSE and MSE values of ERT were the lowest among the three models, which were 0.42 and 0.41, respectively. In clusters A and C, the overall accuracy of the six models was significantly lower than in other clusters. The performance of different models during the growing season was significantly better than that during the non-growing season. During the growing season, with the increasing time scales of SPEI, the prediction accuracy of the model had a small change and basically tended to be stable.

4.4.2 Model errors in spatial patterns

Fig. 4 shows the spatial pattern of errors between the SPEI predicted by the models and the actual SPEI during the non-growing season. The areas with large errors were mainly concentrated in the eastern and northwestern regions of China. The prediction error obtained by the ERT model was the smallest, followed by H2O.DL, and the prediction error by the ELM was the largest. Based on Figs. 4a, b, c, SPEI1, SPEI3, and SPEI6 were significantly overestimated and the prediction errors were basically between 0.5 and 1. The errors of some points in cluster A and cluster C were >1.0 or <-1.0 (Figs. 4a, c, d, e). Figs. 4c and 4h indicated that the prediction performance of H2O.DL was evidently higher than of ELM. Figs. 4h and 4i showed that the errors of the H2O.DL model in Southwest China were profoundly underestimated, and the prediction errors ranged between -0.25 and -0.5. In general, the ELM and H2O.DL models have relatively large errors in the prediction of SPEI at different time scales in Northwest China. However, the performance of ERT was significantly improved in the prediction of SPEI in Northwest China. Figs. 4k-o showed that the errors of SPEI1, SPEI6, and SPEI9 predicted by the ERT model in Northwest China and the Tibet

Plateau were concentrated between -0.25 and 0.25, and the prediction error of the model significantly reduced.

Fig. 5 shows the prediction errors of SPEI at different time scales obtained by different models during the growing season. In general, in clusters D and E, the prediction errors of different models in the growing season were smaller than those in the non-growing season, and the prediction accuracy of the model significantly improved. ERT, H2O.DL and ELM all accurately predicted SPEI1, and the obtained prediction error was low with the error range between -0.1 to 0.1 (Figs. 5a, f, k). Larger prediction errors obtained by the ELM model were found mainly in northwest and southwest China (Figs. 5a-e). The prediction error of SPEI9 by the H2O.DL model in northwest China significantly reduced, but the prediction results for the southwest region had not been significantly improved. It was found from Figs. 5k-o that the prediction accuracy of SPEI at different time scales by the ERT model was the highest, and the prediction error range was between -0.1 to 0.1. Comparison of the prediction errors for SPEI by different models indicated that the ERT model had the best prediction performance.

4.5. Risk of maize yield reduction in compound dry-hot condition

We used STI and SPEI based on the in-situ observations and the SPEI predicted by models to evaluate the risk of the maize yield reduction from 1961 to 2016 under the compound dry-hot condition. Maize yields in the five provinces of North China Plain (NCP) were analyzed as a case study. The NCP is one of the main agricultural production areas in China (Tao and Zhang, 2010), while maize is most vulnerable to climate change (Tao et al., 2008). Hebei, Shandong, Henan, Jiangsu and Anhui provinces are the main provinces in the NCP for maize production. We compared the predicted SPEI by ERT model and observed SPEI changes during the period from 2002 to 2014 (Fig. 6). Fig. 6 demonstrated consistent changes of the predicted SPEI and the observed SPEI, implying reliable prediction results of SPEI by the ERT model.

4.5.1 Impacts of dry-hot condition on maize yields

The main growing period of maize is usually from June to August (Lobell, 2007). The first-order difference processing was done on the maize yield data and climate data to eliminate the influence of trends on maize yields (Nicholls, 1997; Lobell, 2007). Different combinations of SPEI and STI can represent different environmental conditions for crop growth. Here we first defined three dry-hot conditions (Feng et al., 2019b), i.e. extreme drought and normal temperature conditions (SPEI=-1.6 and STI=0), no drought and extreme high temperature conditions (SPEI=0 and STI=1.6), extreme drought and extreme high temperature conditions (SPEI=-1.6 and STI=1.6). When SPEI=0 or STI=0, it can highlight the impact of individual extreme drought or extreme high temperature on the maize yield.

Taking STI, SPEI and SCI as inputs into the meta-Gaussian model (Equation 8) one can obtain the conditional probability density function (PDF) and the cumulative distribution function (CDF) of the SCI variables under different compound dry-hot conditions. The PDF curves showed the probability that different environmental conditions affected the maize yield. In the study, the three compound dry-hot conditions were introduced into the model, and the PDF curves of the maize yield (Figs. 2a-1, b-1, c-1, d-1, e-1) and the corresponding CDF were obtained (Figs. 3a-1, b-1, c-1, d-1, e-1). The PDF curves given SCI=0 indicated the probability that a certain extreme climatic condition would not reduce the maize yield. The CDF given SCI<0 indicated the probability of a certain extreme climatic condition leading to a reduction in maize yield. Comparison of the PDF and CDF curves of different provinces indicated that similar compound dry-hot condition hade various effects on the maize yield, while, with the change of compound dry-hot condition, the PDF and CDF curves of SCI in Henan, Hebei, and Shandong provinces followed similar changes, implying similar probabilities of the maize yield reduction. In Hebei, Henan and Shandong provinces, when SPEI=-1.6 and STI=1.6, the mean values of the SCI probability density function were the smallest, which were -0.51, -0.43 and -0.73, respectively, implying larger probability of the maize yield reduction under the compound dry-hot condition than under one extreme condition (extreme high temperature or extreme drought). We attempted to address the impacts of extreme conditions on the maize yields by modifying one and/or more controlling variables. Given dry-hot conditions from SPEI=-1.6/STI=0 to SPEI=-1.6/STI=1.6, the mean values of the probability corresponding to SCI moved to the left (Figs. 2a-1, d-1, e-1), and the CDF curve shifted upwards (Figs. 2a-2, d-2, e-2), indicating that when air temperature increased, the probability of the maize yield would increase. Specifically, we observed the largest changes in the mean values of the probability relevant to SCI in the Shandong province, being from -0.45 to -0.73, indicating that the maize production in the Shandong province was more influenced by extreme high temperatures. It can be seen from Figs. 7a-1, d-1, and e-1 that when the dry-hot conditions shifted from SPEI=0/STI=1.6 to SPEI=-1.6/STI=0, the probability of maize yield reduction increased. In general, the probability of maize yield reduction in Henan, Hebei and Shandong provinces increased as drought and high temperature conditions intensified. In Jiangsu and Anhui provinces, when SPEI=0/STI=1.6, the SCI by the meta-Gaussian model was the smallest, which was -0.9 and -0.41, respectively, showing that the probability of maize yield reduction reached the maximum under extreme high temperature conditions, and the risk of maize yield reduction was the greatest. Figs. 2b-1, c-1 indicated that extreme drought conditions did not necessarily reduce the maize yield, which can be attributed to mitigation of droughts such as agricultural irrigation. Comparing the CDF curves for different provinces considered in this study, we found that when SCI=0, the corresponding CDF values were all above 0.5, indicating that the probability of maize yield reduction due to extreme high temperatures reached as high as 50%.

4.5.2 Risk of maize yield reduction in different provinces

Different combinations of dry and hot can have variable impacts on maize yields. We defined SPEI=-0.8, -1, 3, and -1.6 as moderate, severe, and extreme droughts. Similarly, we defined STI=0.8, 1.3, and 1.6, respectively, as moderate, high and extremely high temperatures (Feng et al., 2019b). The conditional probability of SCI<0 by the meta-Gaussian model under different compound dry-hot conditions was used to quantify the risk of maize yield reduction due to compound dry-hot condition. Fig. 8 shows the calculated conditional probability of SCI<0 in different provinces under different compound dry-hot conditions. It can be seen from Figs. 8a-e that the risk of the reduced maize production gradually increased with the intensification of compound dry-hot condition in all provinces. In Anhui, when SPEI=-1.6/STI=1.6, the conditional probability of SCI<0 was 0.6. Given shift from SPEI=-0.8/STI=0.8 to SPEI=-1.6/STI=1.6, the probability of maize yield reduction changed from 55% to 60%, and the probability increased by about 5% (Fig. 8a). In Shandong Province, the extreme compound dry-hot conditions had led to the greatest risk of maize yield reduction of higher than 80%. Given the shift from SPEI=-0.8/STI=0.8 to SPEI=-1.6/STI=1.6, the probability of maize yield reduction changed from 66% to 80%, and the probability increased by about 14% (Fig. 8e). In other provinces considered in this study, the combined effects of compound dry-hot conditions caused the maximum probability of 71% for the maize yield reduction (Fig. 8b).

We computed the conditional probability of SCI<0 under the three compound conditions as shown in Fig. 7 to quantify the impacts of droughts or heat hazards on maize yield (Figs. 8f-j). Comparison of Figs. 8i and 8d shows that the high temperature environment in Jiangsu Province would reduce the maize yield, and the extreme high temperature had the greatest impact on maize yield. Given SPEI=0/STI=1.6, the probability of maize yield reduction in Jiangsu Province reached 86%, which was higher than the probability of maize yield reduction under extreme high temperature and extreme drought conditions. A similar phenomenon was also observed in the Anhui

Province. Extremely high temperature caused the probability of 66% of the maize yield reduction, implying that the impact of extreme high temperature on the maize yield was greater than the impact of extreme drought and high temperature on the maize yield in these two provinces. Comparison of Figs. 8b and 8g showed that in Hebei Province, given the shift from SPEI=-0.8/STI=0.8 to SPEI=0/STI=1.6, the probability of maize yield reduction changed from 61% to 57%, implying that the moderate drought-high temperature compound condition had a greater impact on the maize yield than the extreme high temperature only. The compound dry-hot condition had a greater adverse effect on the maize yield changes. In Henan Province, given the shift from SPEI=-1.3/STI=1.3 to SPEI=-1.6/STI=0, the probability of maize yield reduction did not change, indicating that the impact of compound dry-hot condition on the maize yield was similar to that of extreme drought alone on the maize yield variations. In Shandong Province, when SPEI=-1.3/STI=1.3, the probability of maize yield reduction was 75%, while the probability of maize yield reduction under extreme high temperature and extreme drought conditions was 62% and 70%, respectively. It showed that the yield reduction probability of maize under the compound dry-hot conditions of severe drought and high temperature was greater than that under a certain one extreme event. Generally speaking, under the compound conditions of extremely high temperature and extreme drought, the probability of maize yield reduction had reached >60%. It showed that crops were greatly affected by environmental stresses, such as high temperature and precipitation during the growth process, which would eventually have an important impact on the maize yield.

5. Brief discussion

Identification of factors affecting drought and evaluation of drought characteristics have been widely discussed in recent years (Rhee et al., 2010; Park et al., 2016; Feng et al., 2019a; Zuo et al., 2019). The effective identification of drought factors can improve drought monitoring (Zhang et al., 2017b). Park et al. (2016) used the Random Forests, Boosted Regression Trees, and Cubist to analyze the relative impacts of 16 drought influencing factors for SPI at different scales during the growing season. Here we used the GBM to quantify the relative importance of 23 influencing factors for SPEI at different time scales and screened out 10 critical influencing factors. Based on ERT, H2O.DL, and ELM, we compared the prediction accuracy of models before and after the selection of drought factors. We found that the relative importance of NDWI7 increased during the growing season with increasing time scale of SPEI, which is consistent with the findings by Park et al. (2016). Feng et al. (2019a) showed that vegetation was sensitive to drought at 3-month time scale. Therefore, the effective vegetation index is an important variable reflecting the characteristics of drought during the growing season. However, these studies did not show different effects of influencing factors on drought characteristics due to seasonality. We observed high sensitivity of SPEI1 to snow cover changes in the Qinghai-Tibet Plateau and Inner Mongolia, which indicated that snow in winter alleviate drought intensity, and also connections between snow cover and soil moisture. In addition, we also found high correlation between LSWI and SCF. Verbyla (2015) also found high correlation between winter snowfall and summer NDVI in high-altitude areas. It can be speculated that the snowfall in winter or spring may affect vegetation changes and hence the occurrence of droughts.

We used the predicted SPEI to study the probability of maize yield reduction in the main provinces of the NCP under the compound dry-hot conditions. Feng et al. (2019b) used SPI and STI to assess the probability of maize yield reduction in different countries under compound dry-hot conditions and found that the probability of maize yield reduction caused by compound dry-hot conditions in any country was greater than that due to extreme high temperature or dry conditions. When compared to SPI, SPEI was a better choice in reflecting the impact of drought on agricultural, hydrological, and ecological changes (Vicente-Serrano et al., 2012). Using SPEI, we found that in some provinces, such as Anhui and Jiangsu,, the probability of maize yield reduction under extreme high temperature was greater than that due to extreme drought and extreme high temperature. This finding indicated that drought may not necessarily reduce crop yield.

6. Conclusions

Based on remotely sensed data, we investigated the relative importance of 23 drought factors for droughts at different time scales across China. We also compared the performance and reliability of different machine learning models. Meanwhile, we used the predicted drought to evaluate the possibility of maize yield reduction under compound dry-hot conditions. We obtained the following findings:

(1) Based on the FCM, we subdivided China into different regions with different dry

conditions. Meanwhile, we investigated the relative importance of drought factors for different time scales of SPEI during growing and non-growing seasons. We found that soil moisture and precipitation are important variables for assessing drought at different time scales. During the growing season, NDWI7 showed relatively high importance for SPEI at different time scales in different clusters, being up to 70%. LST showed relatively higher importance for short-term drought. During the non-growing season, the snow cover changes showed a relatively high importance for short-term droughts in the Qinghai-Tibet Plateau, Inner Mongolia and the Loess Plateau. LST, NDWI7 and NDDI7 were also important variables for evaluating short-term drought during the non-growing season.

(2) Based on the relative importance of drought factors for different time scales of SPEI, we screened out ten important variables for droughts. We used three machine learning methods, i.e. ERT, H2O.DL, and ELM, to evaluate the prediction accuracy of SPEI before and after selection of drought factors. We found similar prediction accuracy of each model before and after the selection of the drought factors, verifying the reliability of the selected variables. Comparison of the prediction accuracy of different models, we found that the model based on ERT had the highest prediction performance, followed by H2O.DL. Besides, the prediction error range of the ERT model in each region was around -0.1 to 0.1, showing reliable and accurate prediction performance of ERT. This finding provides a theoretical basis for the applicability of ERT for the prediction of drought.

(3) Based on SPEI and STI, we evaluated the risk of maize yield reduction under

compound dry-hot conditions. For the maize yield in Shandong, Henan and Hebei provinces, the intensification of compound dry-hot conditions greatly pushed up the probability of maize yield reduction. Specifically, when SPEI=-1.6/STI=1.6, under the extreme drought and extreme high temperature conditions, the probability of maize yield reduction in Shandong Province reached 80%. When SPEI=0/STI=1.6, under the extreme high temperature conditions, the probability of maize yield reduction in Jiangsu Province reached 86%. This finding provided a theoretical framework for the evaluation of risk of crop yield changes due to different extreme weather and hydrological conditions in other regions of the globe.

Acknowledgments: This research has been financially supported by the China National Key R&D Program, Grant No. 2019YFA0606900, the National Science Foundation of China, Grant No. 41771536, and the National Science Foundation for Distinguished Young Scholars of China, Grant No. 51425903. All authors declare no conflict of interest.

References:

AghaKouchak, A., Nakhjiri, N., 2012. A near real-time satellite-based global drought climate data record. Environ Res Lett, 7(4), 044037.

AghaKouchak, A., Farahmand, A., Melton, F. S., et al., 2015. Remote sensing of drought: Progress, challenges and opportunities. Rev Geophys, 53(2), 452-480.

Alizadeh, M. R., Nikoo, M. R., 2018. A fusion-based methodology for meteorological drought estimation using remote sensing data. Remote Sens Environ, 211, 229-247.

Bajgain, R., Xiao, X., Wagle, P., Basara, J., Zhou, Y., 2015. Sensitivity analysis of vegetation indices to drought over two tallgrass prairie sites. ISPRS J Photogramm Remote Sens, 108, 151-160.

Belayneh, A., Adamowski, J., Khalil, B., Ozga-Zielinski, B., 2014. Long-term SPI drought forecasting in the Awash River Basin in Ethiopia using wavelet neural network and wavelet support vector regression models. J. Hydrol, 508, 418-429.

Bezdek, J.C., 1981. Pattern Recognition with Fuzzy Objective Function Algorithms.Plenum Press, New York.

Campello R.J.G.B., Hruschka E.R., 2006. A fuzzy extension of the silhouette width criterion for cluster analysis. Fuzzy Sets Syst, 157, 2858-2875.

Candel, A., Parmar, V., LeDell, E., Arora, A., 2016. Deep learning with H2O. H2O. ai Inc.

Dai, A., Trenberth, K. E., Qian, T., 2004. A global dataset of Palmer Drought Severity Index for 1870–2002: Relationship with soil moisture and effects of surface warming. J. Hydrometeorol, 5(6), 1117-1130.

Dalin, C., Qiu, H., Hanasaki, N., Mauzerall, D. L., Rodriguez-Iturbe, I., 2015. Balancing water resource conservation and food security in China. Proc Natl Acad Sci, 112(15), 4588-4593.

Dave, R.N., 1996. Validating fuzzy partitions obtained through c-shells clustering. Pattern Recognit Lett, 17, 613-623.

Dunn, J. C., 1973. A fuzzy relative of the ISODATA process and its use in detecting compact well-separated clusters. doi: 10.1080/01969727308546046

Faiz, M. A., Liu, D., Tahir, A. A., et al., 2020. Comprehensive evaluation of 0.25° precipitation datasets combined with MOD10A2 snow cover data in the ice-dominated river basins of Pakistan. Atmos Res, 231, 104653.

Feng, P., Wang, B., Li Liu, D., Yu, Q., 2019a. Machine learning-based integration of remotely-sensed drought factors can improve the estimation of agricultural drought in South-Eastern Australia. Agric Syst, 173, 303-316.

Feng, S., Hao, Z., Zhang, X., Hao, F. 2019b. Probabilistic evaluation of the impact of compound dry-hot events on global maize yields. Sci Total Environ, 689, 1228-1234.

Friedman, J. H., 2001. Greedy function approximation: a gradient boosting machine. Ann Stat, 29(5), 1189-1232.

Friedman, J. H., 2002. Stochastic gradient boosting. Comput Stat Data Anal, 38(4), 367-378.

Hayes, M. J., Alvord, C., Lowrey, J., 2007. Drought indices. Intermountain west climate summary, 3(6), 2-6.

Hao C, Zhang J, Yao F., 2015. Combination of multi-sensor remote sensing data for drought monitoring over southwest china. Int J Appl Earth Obs Geoinf, 35, 270-283.

Huang, G. B., Zhu, Q. Y., Siew, C. K., 2006. Extreme learning machine: theory and applications. Neurocomputing, 70 (1-3), 489-501.

Huang, G., Song, S., Gupta, J. N., Wu, C., 2014. Semi-supervised and unsupervised extreme learning machines. IEEE Trans Cybern, 44 (12), 2405-2417.

Gao, B. C., 1996. NDWI—A normalized difference water index for remote sensing of vegetation liquid water from space. Remote Sens Environ, 58(3), 257-266.

Geurts, P., Ernst, D., Wehenkel, L., 2006. Extremely randomized trees. Mach Learn, 63 (1), 3-42.

Guzmán, S. M., Paz, J. O., Tagert, M. L. M., Mercer, A. E., Pote, J. W., 2018. An integrated SVR and crop model to estimate the impacts of irrigation on daily groundwater levels. Agric Syst, 159, 248-259.

Gu, Y., Brown, J. F., Verdin, J. P., Wardlow, B., 2007. A five-year analysis of MODIS NDVI and NDWI for grassland drought assessment over the central Great Plains of the United States. Geophys Res Lett, 34(6).

Guan, B., Molotch, N. P., Waliser, D. E., et al., 2013. Snow water equivalent in the Sierra Nevada: Blending snow sensor observations with snowmelt model simulations. Water Resour Res, 49(8), 5029-5046.

Gupta, S., Arango-Argoty, G., Zhang, L., Pruden, A., Vikesland, P., 2019. Identification of discriminatory antibiotic resistance genes among environmental resistomes using extremely randomized tree algorithm. Microbiome, 7(1), 123.

Guo, H., Bao, A., Liu, T., Ndayisaba, F., et al., 2019. Determining variable weights for an Optimal Scaled Drought Condition Index (OSDCI): Evaluation in Central Asia. Environ Res Lett, 231, 111220.

Kaufman L., Rousseeuw P.J., 1990. Finding Groups in Data: An Introduction to Cluster

Analysis. Wiley, New York.

Kelly, K. S., Krzysztofowicz, R., 1997. A bivariate meta-Gaussian density for use in hydrology. Stochastic Hydrology and hydraulics, 11 (1), 17-31.

Kogan, F. N., 1995. Application of vegetation index and brightness temperature for drought detection. Adv Space Res, 15(11), 91-100.

Knox, J. W., Weatherhead, E. K., Bradley, R. I., 1997. Mapping the total volumetric irrigation water requirements in England and Wales. Agric Water Manag, 33(1), 1-18.

Leng, G., Hall, J., 2019. Crop yield sensitivity of global major agricultural countries to droughts and the projected changes in the future. Sci Total Environ, 654, 811-821.

Lillesand, T., Kiefer, R. W., Chipman, J., 2015. Remote sensing and image interpretation. John Wiley & Sons.

Li, T., Shen, H., Yuan, Q., Zhang, X., Zhang, L., 2017. Estimating ground-level PM2. 5 by fusing satellite and station observations: a geo-intelligent deep learning approach. Geophys Res Lett, 44 (23), 11-985.

Lu, J., Carbone, G. J., Gao, P., 2019. Mapping the agricultural drought based on the long-term AVHRR NDVI and North American Regional Reanalysis (NARR) in the United States, 1981–2013. Appl Geogr, 104, 10-20.

Lobell, D. B., 2007. Changes in diurnal temperature range and national cereal yields. Agric For Meteorol, 145 (3-4), 229-238.

Marée, R., Geurts, P., Wehenkel, L., 2007. Random subwindows and extremely randomized trees for image classification in cell biology. BMC Cell Biol, 8 (1), 1-

12.

Machado, G., Mendoza, M. R., Corbellini, L. G., 2015. What variables are important in predicting bovine viral diarrhea virus? A random forest approach. Vet Res, 46 (1), 85.

McKee T B, Doesken N J, Kleist J., 1993. The relationship of drought frequency and duration to time scales. In Proceedings of the 8th Conference on Applied Climatology (Vol. 17, No. 22, pp. 179-183).

Molotch, N. P., Margulis, S. A., 2008. Estimating the distribution of snow water equivalent using remotely sensed snow cover data and a spatially distributed snowmelt model: A multi-resolution, multi-sensor comparison. Adv Water Resour, 31(11), 1503-1514.

Nicholls, N., 1997. Increased Australian wheat yield due to recent climate trends. Nature, 387 (6632), 484-485.

Palmer W C. Meteorological drought. Research Paper No. 45. Washington, DC: US Department of Commerce. Weather Bureau, 1965.

Park, S., Im, J., Jang, E., Rhee, J., 2016. Drought assessment and monitoring through blending of multi-sensor indices using machine learning approaches for different climate regions. Agric For Meteorol, 216, 157-169.

Pumsirirat, A., Yan, L., 2018. Credit card fraud detection using deep learning based on auto-encoder and restricted boltzmann machine. Int J Adv Comput Sci Appl, 9 (1), 18-25.

Ray, D. K., Gerber, J. S., Macdonald, G. K., West, P. C. 2015. Climate variation explains a third of global crop yield variability. Nat Commun, 6(1), 5989-5989.

Rao, A. R., Srinivas, V. V., 2006. Regionalization of watersheds by fuzzy cluster analysis. J. Hydrol, 318 (1-4), 57-79.

Rao, H., Shi, X., Rodrigue, A. K., Feng, J., Xia, Y., Elhoseny, M., Yuan, X., Gu, L., 2019. Feature selection based on artificial bee colony and gradient boosting decision tree. Appl Soft Comput, 74, 634-642.

Rajesh, R., Prakash, J. S., 2011. Extreme learning machines-a review and state-of-the-art. International journal of wisdom based computing, 1(1), 35-49.

Rhee, J., Im, J., Carbone, G. J., 2010. Monitoring agricultural drought for arid and humid regions using multi-sensor remote sensing data. Remote Sens Environ, 114 (12), 2875-2887.

Rouse, J. W., Haas, R. H., Schell, J. A., Deering, D. W., 1974. Monitoring vegetation systems in the Great Plains with ERTS. NASA special publication, 351, 309.

Rodriguez, J. D., Perez, A., Lozano, J. A., 2009. Sensitivity analysis of k-fold cross validation in prediction error estimation. IEEE Trans Pattern Anal Mach Intell, 32 (3), 569-575.

Sayago, S., Ovando, G., Bocco, M., 2017. Landsat images and crop model for evaluating water stress of rainfed soybean. Remote Sens Environ, 198, 30-39.

Sun, P., Q. Zhang, Q. Wen, V.P. Singh, P. Shi, 2017. Multisource data based integrated agricultural drought monitoring in the Huai River basin, China. J Geophys Res, 122, 10751-10772.

Stewart, C., 2017.Detection of Archaeological Residues in Vegetated Areas Using

Satellite Synthetic Aperture Radar. Remote Sens, 9, 118.

Tao, F., Yokozawa, M., Liu, J., Zhang, Z., 2008. Climate–crop yield relationships at provincial scales in China and the impacts of recent climate trends. Clim Res, 38 (1), 83-94.

Tao, F., Zhang, Z., 2010. Adaptation of maize production to climate change in North China Plain: quantify the relative contributions of adaptation options. Eur J Agron, 33 (2), 103-116.

Tuv, E., Borisov, A., Runger, G., Torkkola, K., 2009. Feature selection with ensembles, artificial variables, and redundancy elimination. J Mach Learn Res, 10 (Jul), 1341-1366.

Wilhite, D. A., Glantz, M. H., 1985. Understanding: the drought phenomenon: the role of definitions. Water Int, 10(3), 111-120.

Wilks, D. S., 2011. Statistical methods in the atmospheric sciences (Vol. 100). Academic press.

Wang, H., Vicente-Serrano, S. M., Tao, F., et al., 2016. Monitoring winter wheat drought threat in Northern China using multiple climate-based drought indices and soil moisture during 2000–2013. Agric For Meteorol, 228, 1-12.

Wang, L., Qu, J. J., 2007. NMDI: A normalized multi-band drought index for monitoring soil and vegetation moisture with satellite remote sensing. Geophys Res Lett, 34(20).

Xie X.L., Beni G., 1991. A validity measure for fuzzy clustering, IEEE Trans Pattern Anal Mach Intell, 13, 841-847.

Xiao, X., Hollinger, D., Aber, J., Goltz, M., Davidson, E. A., Zhang, Q., Moore III, B., 2004. Satellite-based modeling of gross primary production in an evergreen needleleaf forest. Remote Sens Environ, 89(4), 519-534.

Verbyla, D., 2015. Remote sensing of interannual boreal forest NDVI in relation to climatic conditions in interior Alaska. Environ Res Lett, 10(12), 125016.

Vicente-Serrano S M, Beguería S, López-Moreno J I.,2010. A multiscalar drought index sensitive to global warming: the standardized precipitation evapotranspiration index. J Clim, 23(7), 1696-1718.

Vicente-Serrano, S. M., Beguería, S., Lorenzo-Lacruz, J., Camarero, J. J., López-Moreno, J. I., Azorin-Molina, C., Revuelto, J; Morán-Tejeda, E Sanchez-Lorenzo, A., 2012. Performance of drought indices for ecological, agricultural, and hydrological applications. Earth Interact, 16 (10), 1-27.

Yu, H., Q. Zhang, C.-Y. Xu, J. Du, P. Sun, P. Hu, 2019. Modified Palmer Drought Severity Index: model improvement and application. Environ Int, 130, 104951.

Zambrano, F., Vrieling, A., Nelson, A., Meroni, M., Tadesse, T., 2018. Prediction of drought-induced reduction of agricultural productivity in Chile from MODIS, rainfall estimates, and climate oscillation indices. Remote Sens Environ, 219, 15-30.

Zuo, D., Cai, S., Xu, Z., et al., 2019. Assessment of meteorological and agricultural droughts using in-situ observations and remote sensing data. Agric Water Manag, 222, 125-138.

Zhou, Y., Xiao, X., Zhang, G., et al., 2017. Quantifying agricultural drought in tallgrass prairie region in the US Southern Great Plains through analysis of a water-related vegetation index from MODIS images. Agric For Meteorol, 246, 111-122.

Zhang, A., Jia, G., 2013. Monitoring meteorological drought in semiarid regions using multi-sensor microwave remote sensing data. Remote Sens Environ, 134, 12-23.

Zhang, Q., H. Yu, P. Sun, V.P. Singh, P. Shi, 2019. Multisource data based agricultural drought monitoring and agricultural loss in China. Glob Planet Change, 172, 298-306.

Zhang, Q., Q. Li, V.P. Singh, P. Shi, Q. Huang, P. Sun, 2018. Nonparametric integrated agrometeorological drought monitoring: model development and application. J Geophys Res, 123, 73-88.

Zhang, X., Chen, N., Li, J., Chen, Z., Niyogi, D., 2017a. Multi-sensor integrated framework and index for agricultural drought monitoring. Remote Sens Environ, 188, 141-163.

Zhang, L., Jiao, W., Zhang, H., Huang, C., Tong, Q., 2017b. Studying drought phenomena in the Continental United States in 2011 and 2012 using various drought indices. Remote Sens Environ, 190, 96-106.

Zhang, X., Waller, S. T., Jiang, P., 2020. An ensemble machine learning-based modeling framework for analysis of traffic crash frequency. Computer-Aided Civil and Infrastructure Engineering, 35 (3), 258-276.

Zhang, Y., Haghani, A., 2015. A gradient boosting method to improve travel time prediction. Transp Res Part C Emerg Technol, 58, 308-324.

Zscheischler, J., Michalak, A. M., Schwalm, C., Mahecha, M. D., et al., 2014. Impact of large-scale climate extremes on biospheric carbon fluxes: An intercomparison based on MsTMIP data. Global Biogeochem Cycles, 28 (6), 585-600.

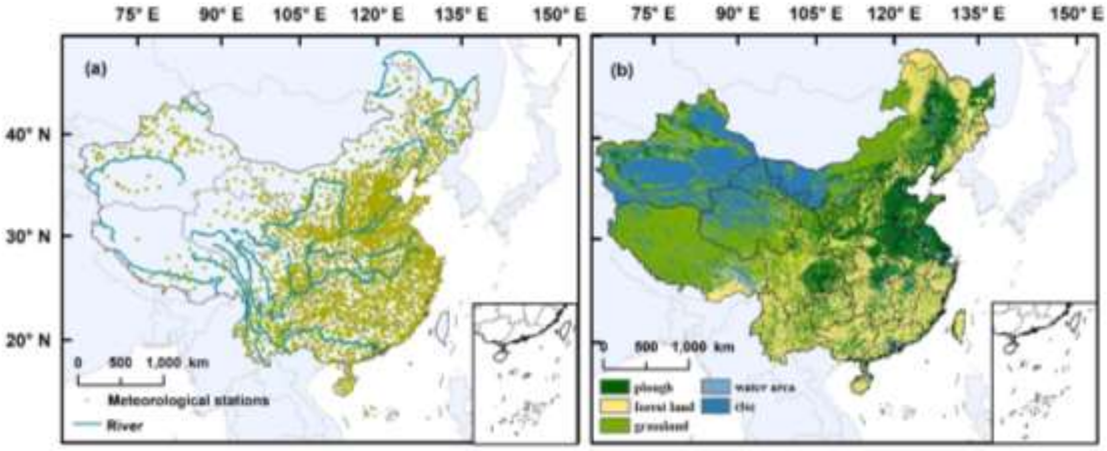

Fig. 1. Spatial distributions of meteorological stations (a) and land cover types (b) across China.

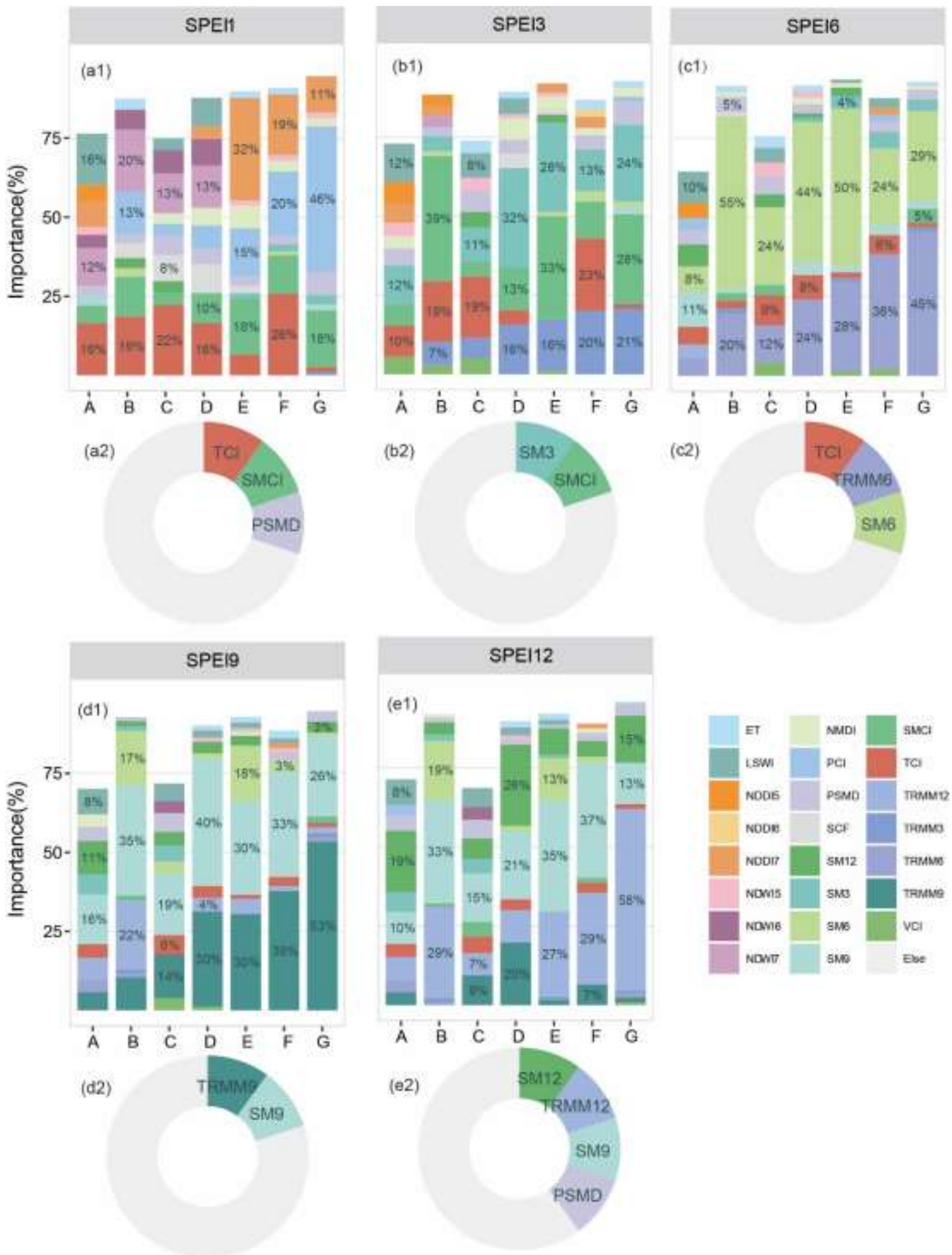

Fig. 2. The relative importance (a1, b1, c1, d1, e1) and the frequency (a2, b2, c2, d2, e2) of the most important ten input variables in each cluster for SPEI forecasts with 1-, 3-, 6-, 9-, and 12-month different time-scales derived by GBT and during non-crop seasons.

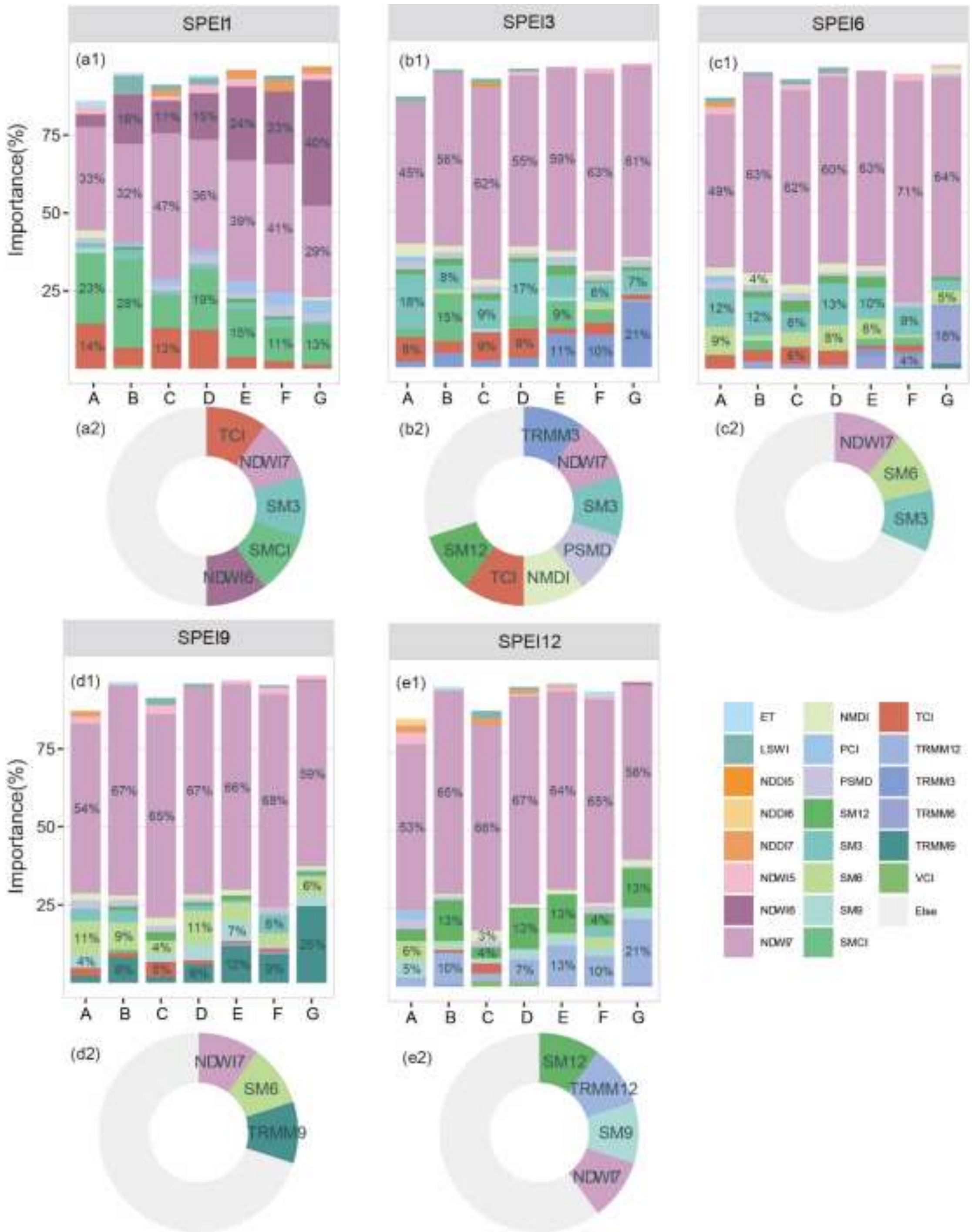

Fig. 3. The relative importance (a1, b1, c1, d1, e1) and the frequency (a2, b2, c2, d2, e2) of the most important ten input variables in each cluster for SPEI forecasts with 1-, 3-, 6-, 9-, and 12-month different time-scales derived by GBT and during crop seasons.

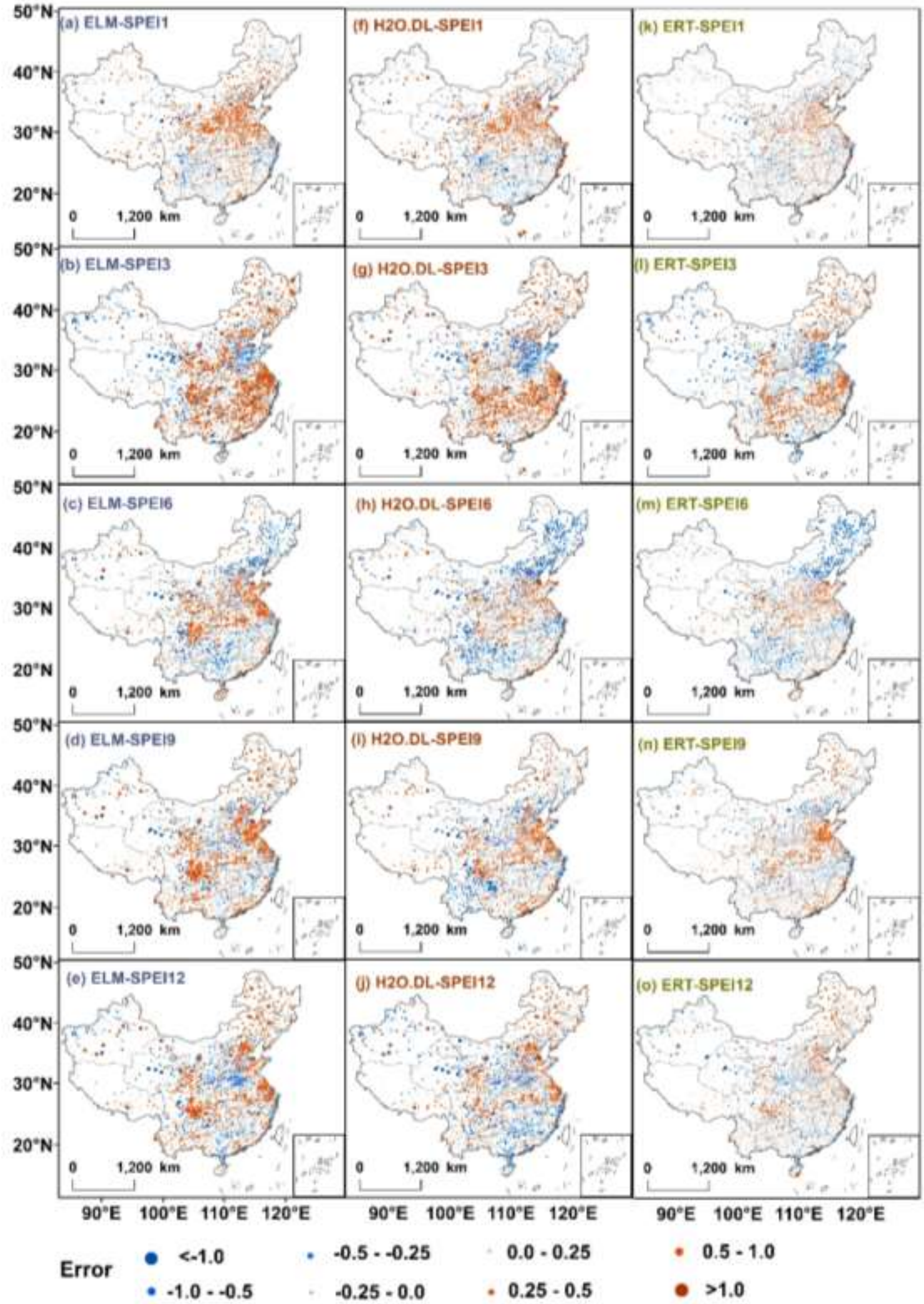

Fig. 4. Spatial patterns of the error of SPEI with 1-, 3-, 6-, 9-, and 12-month different time-scales by the models during non-crop seasons. (a) - (e) derived by ELM; (f) - (j) derived by H2O.DL; (k) - (o) derived by ERT. The error is the difference between the estimated SPEI and the in situ observed SPEI.

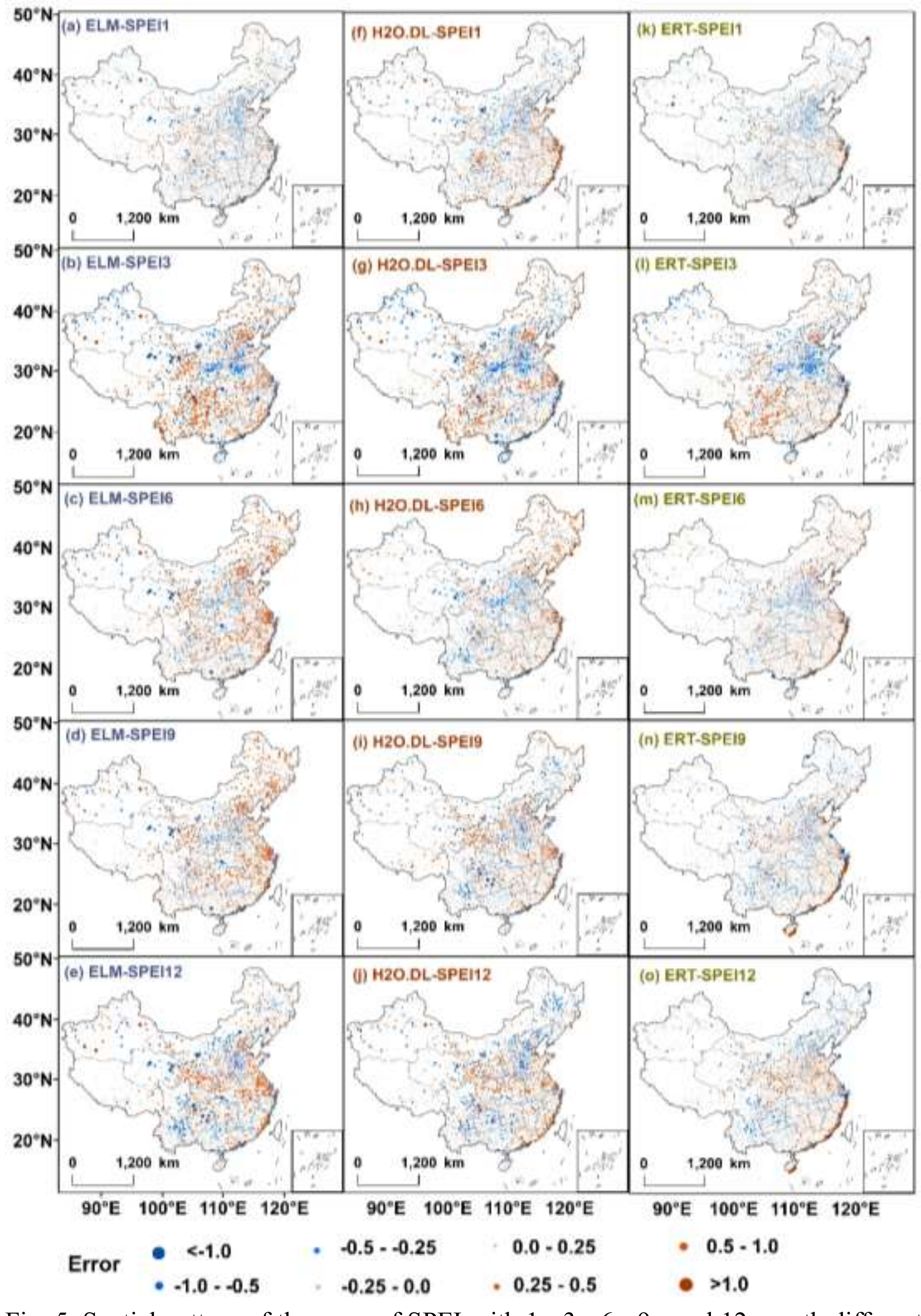

Fig. 5. Spatial pattern of the error of SPEI with 1-, 3-, 6-, 9-, and 12-month different time-scales by the models during crop seasons. (a) - (e) derived by ELM; (f) - (j) derived by H2O.DL; (k) - (o) derived by ERT. The error is the difference between the estimated SPEI and the in situ observed SPEI.

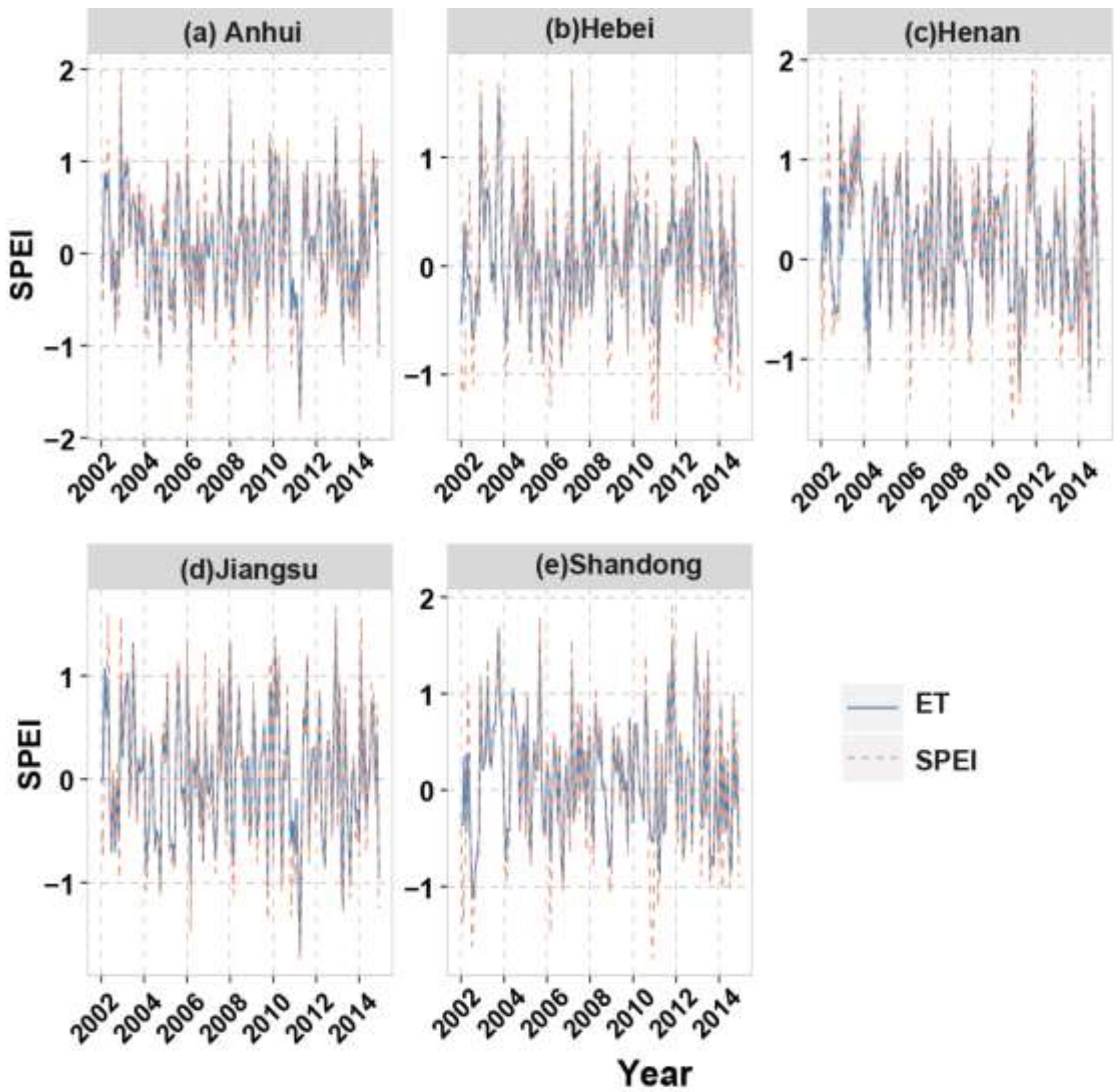

Fig. 6. The trend of the estimated SPEI by ERT and the in situ observed SPEI in different regions during 2002-2014.

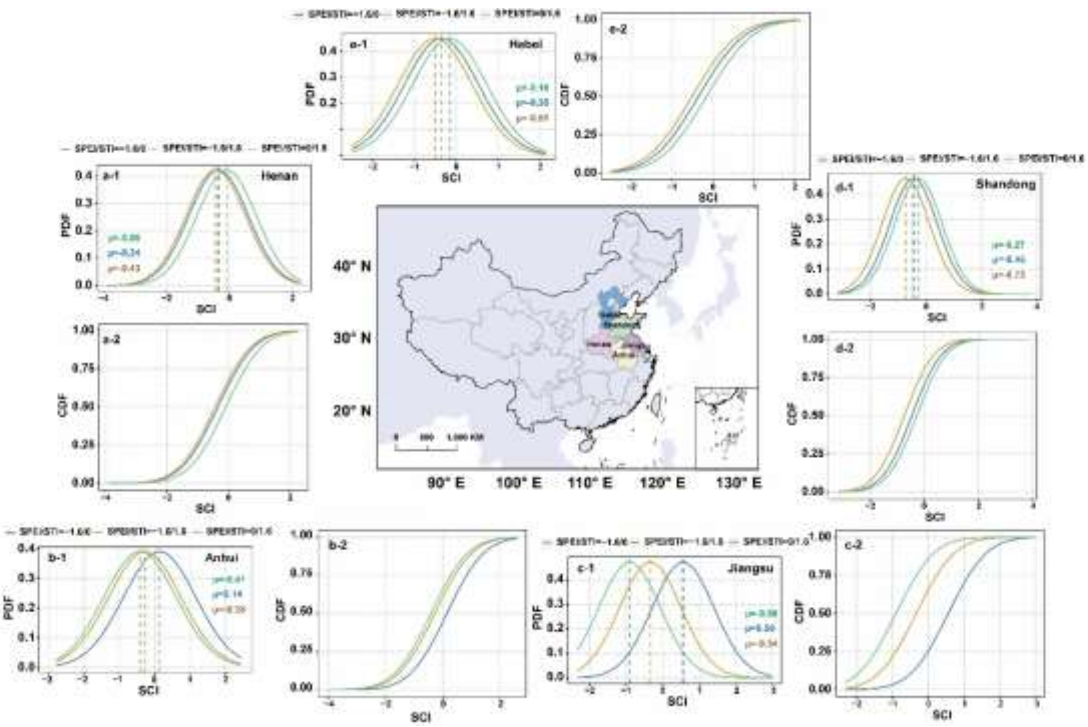

Fig. 7. The conditional PDF and CDF of SCI of maize given three compound conditions in Henan (a-1, a-2), Anhui (b-1, b-2), Jiangsu (c-1, c-2), Shandong (d-1, d-2) and Hebei (e-1, e-2) provinces.

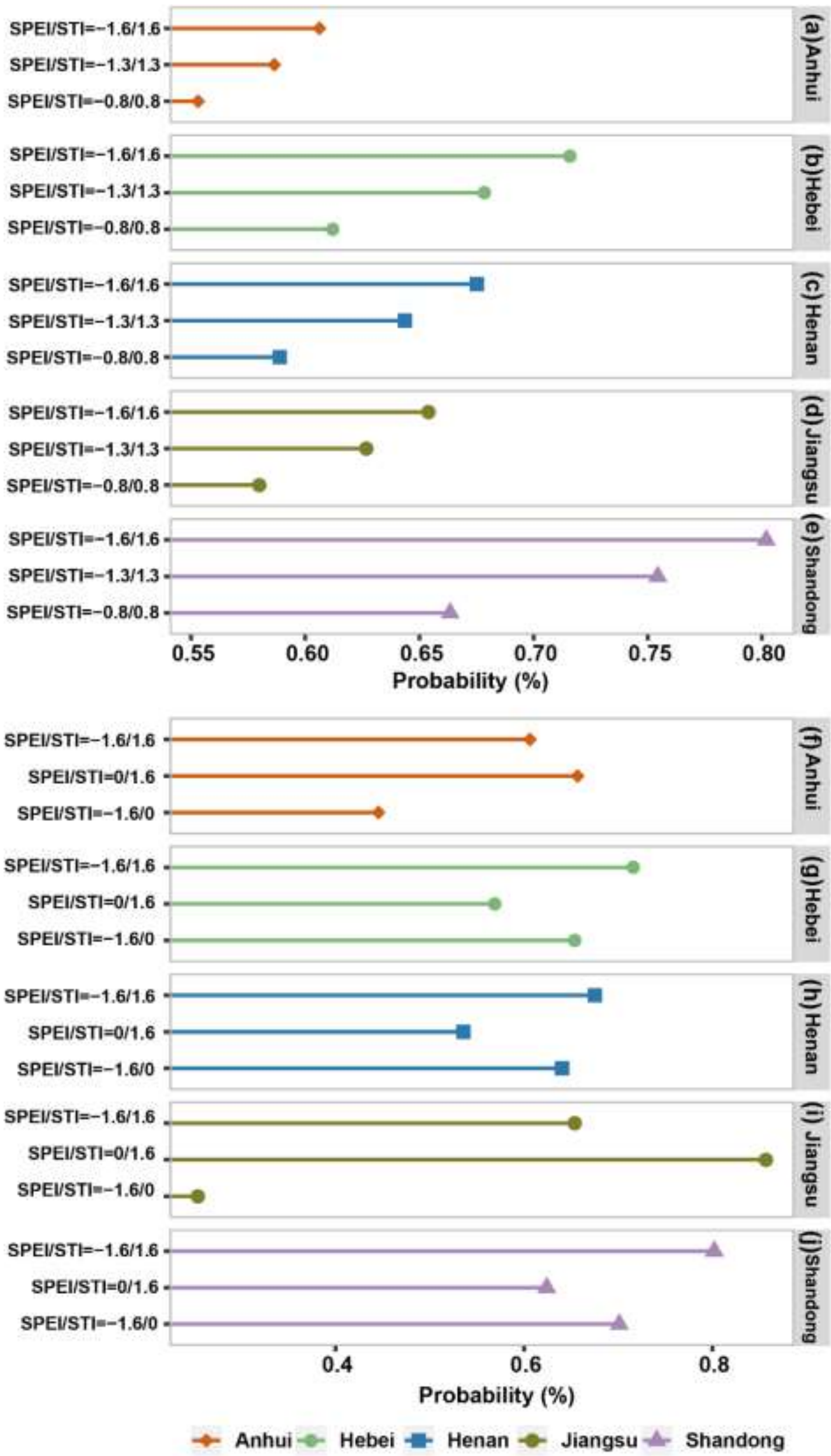

Fig. 8. The conditional probability of SCI<0 given different compound conditions in five provinces.

Table 1 Descriptions of drought factors.

Drought factors	Formula	References
NDWI5. 6. 7	$(\rho_{\text{band2}} - \rho_{\text{band5(or 6 or 7)}})/(\rho_{\text{band2}} + \rho_{\text{band5(or 6 or 7)}})$	Gao (1996)
NMDI	$(\rho_{\text{band2}} - (\rho_{\text{band6}} - \rho_{\text{band7}}))/(\rho_{\text{band2}} + (\rho_{\text{band6}} - \rho_{\text{band7}}))$	Wang and Qu (2007)
NDDI5, 6, 7	$(\text{NDVI} - \text{NDWI})/(\text{NDVI} + \text{NDWI})$	Gu (2007)
LSWI	$(\rho_{\text{band2}} - \rho_{\text{band6}}))/(\rho_{\text{band2}} + \rho_{\text{band6}})$	Zhou et al. (2017)
VCI	$(\text{NDVI} - \text{NDVI}_{\text{min}})/(\text{NDVI}_{\text{max}} - \text{NDVI}_{\text{min}})$	Kogan (1995)
TCI	$(\text{LST}_{\text{max}} - \text{LST})/(\text{LST}_{\text{max}} - \text{LST}_{\text{min}})$	Kogan (1995)
PCI	$(\text{TRMM} - \text{TRMM}_{\text{min}})/(\text{TRMM}_{\text{max}} - \text{TRMM}_{\text{min}})$	Du et al (2013)
SMCI	$(\text{SM} - \text{SM}_{\text{min}})/(\text{SM}_{\text{max}} - \text{SM}_{\text{min}})$	Zhang and Jia (2013)
Scaled ET	$(\text{ET} - \text{ET}_{\text{min}})/(\text{ET}_{\text{max}} - \text{ET}_{\text{min}})$	Park et al. (2016)
PSMD_i	$(\text{PSMD}_{i-1} + \text{PET}_i - \text{P}_i)$	Stewart (2017)

Table 2 Four cluster validity indices of FCM cluster

Names of Index	Formula	References
Modified partition coefficient (MPC)	$\mathrm{MPC(c)} = 1 - \frac{c}{c-1}(1 - \frac{1}{n}\sum_{i=1}^{m}\sum_{j=1}^{n}(u_{ji})^2)$	Dave (1996)
Silhouette index (SIL)	$\mathrm{SIL(c)} = \frac{\min\limits_{h}[\frac{1}{n_h}\sum_{y\in c_h} d(x,y)] - \frac{1}{n_k - 1}[\sum_{y\in c_k} d(x,y)]}{\max(\min\limits_{h}[\frac{1}{n_h}\sum_{y\in c_h} d(x,y)], \frac{1}{n_k - 1}[\sum_{y\in c_k} d(x,y)])}$	Kaufman (1990)
Fuzzy silhouette index (SIL.F)	$\mathrm{SIL.F(c)} = \frac{\sum_j^n SIL(u_{pj} - u_{qj})^\alpha}{\sum_j^n (u_{pj} - u_{qj})^\alpha}$	Campello (2006)
Xie and Beni index (XB)	$\mathrm{XB(c)} = \frac{\sum_{i=1}^{m}\sum_{j=1}^{n}(u_{ji})^k \lVert X_j - V_i \rVert^2}{n \min\limits_{l} \lVert X_l - V_i \rVert^2}$	Xie and Bein (1991)